Fully Tunable Silicon Nanowire Arrays by Soft Nanoparticle Templating

By Marcel Rey [a,†], Roey Elnathan [b,†], Ran Ditcovski [c], Karen Geisel [d], Michele Zanini [a], Miguel-Angel Fernandez-Rodriguez [a,e], Vikrant V. Naik [f], Andreas Frutiger [g], Walter Richtering [d], Tal Ellenbogen [c], Nicolas. H. Voelcker [b] and Lucio Isa [a,]*

a) Laboratory for Interfaces, Soft Matter and Assembly, Department of Materials, ETH Zurich, Vladimir-Prelog-Weg 5, CH-8093 Zurich, Switzerland

b) ARC Centre of Excellence in Convergent Bio-Nano Science and Technology, Mawson Institute, University of South Australia, Mawson Lakes, 5095, Australia

c) Department, of Physical Electronics, Fleischman Faculty of Engineering, Tel-Aviv University, Tel-Aviv 69978, Israel

d) Institute of Physical Chemistry, RWTH Aachen University, Landoltweg 2, 52056

Aachen, Germany

e) Biocolloid and Fluid Physics Group, Applied Physics, University of Granada, 18071 Granada, Spain

f) Laboratory for Surface Science and Technology, Department of Materials, ETH Zurich, Vladimir-Prelog-Weg 5, CH-8093 Zurich, Switzerland

g) Laboratory of Biosensors and Bioelectronics, Institute for Biomedical Engineering, ETH Zurich, Gloriastrasse 35, ETZ F76, CH-8092 Zurich, Switzerland

KEYWORDS: Vertically aligned nanowires; nanoscale patterning; microgels; fluid interfaces; 2D photonic crystals; optical cavities.

ABSTRACT

We demonstrate a fabrication breakthrough to produce large-area arrays of vertically aligned silicon nanowires (VA-SiNWs) with full tunablity of the geometry of the single nanowires and of the whole array, paving the way towards advanced programmable designs of nanowire platforms. At the core of our fabrication route, termed "Soft Nanoparticle Templating", is the conversion of gradually compressed self-assembled monolayers of soft nanoparticles (microgels) at a water-oil interface into customised lithographical masks to create VA-SiNW arrays by means of metal-assisted chemical etching (MACE). This combination of bottom-up and top-down techniques affords excellent control of nanowire etching site locations, enabling independent control of nanowire spacing, diameter and height in a single fabrication route. We demonstrate the fabrication cm-scale 2D gradient photonic crystals exhibiting continuously varying structural

colors across the entire visible spectrum on a single silicon substrate, and the formation of tunable optical cavities supported by the VA-SiNWs, as unambiguously demonstrated through numerical simulations. Finally, Soft Nanoparticle Templating is combined with optical lithography to create hierarchical and programmable VA-SiNW patterns.

TEXT

Nanoscale patterning is widely used across disciplines to impart new functions and properties to materials. Arrays of vertically-aligned silicon nanowires (VA-SiNWs) are a prominent example, where control of both their crystallographic structure (i.e. growth direction), and of their geometrical parameters (diameter, height and spacing) enables the emergence of different photonic [1-7], electronic [8], mechanical [9], wetting [10] and biointerface properties [11] compared to the bulk material. These include increased optical absorption due to light trapping [12], generation of structural colors due to wave-guiding and resonance phenomena [13], high density of nanowire field-effect transistors (FETs)[8], and the ability to transfect cells *in vitro* and *in vivo* [6,11,14]. Future nanowire-based device technology requires though an economically viable path toward high-throughput, robust, and scalable processing, and ideally the ability to fabricate VA-SiNW arrays with precise control of their geometrical parameters.

Current nanofabrication of VA-SiNW arrays is either based on bottom-up processes, such as vapor–liquid–solid (VLS) [15-17] and metal–organic vapor-phase epitaxy (MOVPE) [18,19] , or top-down methods, such as reactive ion etching (RIE) and metal-assisted chemical etching (MACE) [20-22]. Despite significant research efforts [23], achieving high-resolution, cheap and easy-to-implement fabrication via chemical vapor deposition methods currently remains elusive. In

contrast, better control of the spatial organization of VA-SiNW arrays can be reached using top-down methods combined with lithographic steps. Nearly all existing lithographical technologies, e.g. photolithography, electron beam lithography [24], dip-pen nanolithography [25], and nanoimprint lithography [26] have been used to generate etching masks for VA-SiNW [24,26,27]. In spite of the added flexibility, these processes are either sequential, and thus slow and limited to small areas, or require expensive equipment of limited accessibility.

A promising alternative to these methods is colloidal lithography, namely the controlled deposition of nano or microparticles onto a solid substrate, which act either as a direct mask[28] or are used to produce metal masks complementary to the particle arrangement [29]. The advantages are manifold: the large availability of highly monodisperse particles allows precise control over the feature size, and the process is inherently parallel and scalable to large samples. Yet, the main limitation lies in the accurate control of the spacing between the features. A possible method to create non-close-packed (ncp) patterns of spherical colloids is shrinking close-packed arrays of particles using reactive plasma etching[30], but the size of the original spheres sets the relation between the feature size and spacing, i.e. the two cannot be changed independently and continuously on the same substrate. Alternatively, ncp masks can be obtained by exploiting self-assembly and deposition of charged colloids at fluid-fluid interfaces [31,32], onto nanostructured templates [33] or by deposition on stretchable elastomers[34]. The first method carries limitations over the size range and separation of the colloids, the second one allows exquisite control over the deposited pattern, but requires the fabrication of templates via undesired lithography steps, while the last one is an extremely simple and flexible alternative, but requires some high-

temperature steps, which limit its applicability to inorganic particles (e.g. silica) that cannot be used as MACE masks.

In this work, we show that these obstacles can be completely overcome by using microgel particles. Microgels are soft, compressible nanoparticles consisting of cross-linked, water-soluble polymers, typically showing a more densely cross-linked core surrounded by a looser corona [35,36] (see Figure 1a). This conformation is emphasized when the microgels are confined at an oil-water (o/w) interface, where the corona adsorbs and stretches out to form an extended soft shell around the cores [37] (Figure 1b). Upon spreading and compression at an o/w interface, a range of different structures can be produced [38]. In particular, as the coronas enter into steric contact, the particle cores readily self-assemble into large-area, high-quality 2D ncp hexagonal crystals (Figure 1c), which can be compressed until the particles experience core-core contacts (Figure 1d). However, after deposition and drying, the height of the microgels is only of a few nm, resulting in insufficient material contrast for use as lithography masks. Here we show that a simple modification step solves this problem and enables the novel use of the microgels as lithography masks for the fabrication of fully tunable, large-area optically active VA-SiNW arrays.

The process, that we name "Soft Nanoparticle Templating", is based on the following fabrication steps as described schematically in Figure 1 (full details are in the Methods section of the SI). A monolayer of microgel particles (synthesized as in the Methods section of the SI) is prepared by spreading a controlled volume of a microgel suspension at a water-hexane interface in a customized Langmuir trough by means of a precision micro-syringe. The trough has a custom-made bath to allow simultaneously compression experiments and monolayer deposition from an

o/w interface. A number of microgels is spread so that before starting the compression, the surface pressure is approximately 2-3 mN/m. This corresponds to particles in corona-corona contact that form a hexagonal ncp layer of the cores. After equilibration, the barriers of the Langmuir trough are closed at a speed of 2.3 mm/min and, simultaneously, a silanized 2x1 cm^2 silicon substrate, is raised through the interface at a 30° angle and a speed of 0.3 mm/min, so that it has fully crossed the interface when the compression stops. In this way, we can achieve the complete deposition of an interfacial monolayer at a continuously varying surface pressure/area per particle, *where different positions on the substrate correspond to different compression states of the monolayer*. Upon raising the surface pressure up to 18 mN/m, the corona-corona contacts in the ncp microgel crystal are uniformly compressed and we achieve gradients of distances between the particle cores continuously varying from 550 to 350 nm on the same substrate (from the lowest compression to the highest compression, respectively), while maintaining a highly 2D hexagonal crystalline structure (see Figure 2). Only at the highest surface pressure we observe the formation of small microgel clusters and a weaker dependence of inter-particle spacing on compression. The procedure is highly reproducible and the gradient is only defined by the initial amount of spread particles and by the deposition protocol. Different samples prepared in similar conditions give analogous gradients robustly showing the same properties (see Supplementary Figure S1). The same method can also be used to produce cm^2 microgel arrays with uniform inter-particle separation, by keeping a constant surface pressure during deposition, i.e. by adjusting the trough area, so that all positions on the substrate correspond to the same compression state, as typically done in Langmuir-Blodgett depositions (see Methods section and Figure 3).

After deposition, the microgels are swollen *in situ* using a photoresist. After fixation, the resist is washed first with acetone and then ethanol, and the substrate is dried under a steep angle. Ethanol swells the microgels and the receding drying front leaves behind swollen microgels that incorporate photoresist residues still dissolved in the solvent. Upon complete evaporation of the ethanol, the photoresist remains inside the microgels, leading to an increase in the height profile of the dry particles from 30 nm to 100 nm (more details are in the SI, Supplementary Figures S1, S2 and S3). Finally, the swollen microgels are exposed to oxygen plasma for up to one minute; after 15 seconds of plasma time, the particle corona is removed, and further exposure leads to a controlled reduction of the particle diameter (see Supplementary Figure S4).

The microgel arrays are then sputter-coated by a 10 nm-thick Au layer to produce masks for MACE (details for the etching conditions in the Methods section of the SI). Specifically, the swollen microgels act as spacers between the Au layer and the silicon substrate and, as a consequence, the wafer is etched preferentially around the microgels where the catalytic Au layer is in direct contact with the silicon substrate, causing the formation of VA-SiNWs. The duration of the etching controls the height of the nanowires, while the diameter of the microgel core, tunable by O_2 plasma, defines the nanowire diameter.

Due to the smooth, controlled compression of the interface, these customized masks enable the generation of a gradient of nanowire spacing with the same diameter, on the same substrate, and in a single deposition. This emphasizes the potential and the flexibility of Soft Nanoparticle Templating to produce novel VA-SiNWs platforms, where the geometry of the individual

nanowires and the properties of the array are decoupled and can be robustly, accurately and independently tuned, over cm^2 scales. This feature holds the key to future technological applications and has so far not been demonstrated by any other method.

Figure 2 provides an example of such gradient samples. In Figure 2a, AFM images of the deposited microgels and SEM top-views of the nanowire array after etching at different positions on the substrate are summarized. The different locations correspond to different surface pressures (see Figure 2b for the relation between position and surface pressure). A side view of the array, demonstrating that these nanowires have an aspect ratio of 20, is shown in Figure 2c. The continuous gradient in nanowire spacing causes smoothly changing structural colors of the substrate, covering the entire visible range, as visualized in Figure 2d, and later measured in Figure 5b.

Additionally, as previously described, the diameter of the nanowires can also be independently tuned by shrinking the swollen microgels using an O_2 plasma. Figure 3 shows examples of nanowire arrays with the same center-to-center spacing but with continuously varying radii in the range between 90 and 50 nm. In line with previous findings [3], these substrates also show different colors at normal incidence in reflection mode depending on the nanowire diameter (Figure 3d). The images and data points in Figure 3 have been collected on separate samples prepared independently by depositions at the same constant surface pressure (8 mN/m), demonstrating both the capability of producing cm^2 arrays with controlled uniform pitch and the robustness and reproducibility of the process.

We then proceeded to carefully characterize the remarkable optical properties of the tunable VA-SiNW gradient arrays. Previous reports have described some of the intriguing optical properties of VA-SiNWs[2,3,7,12,13], which depend on the local geometrical parameters of the nanowires, e.g. their size and shape, and on their nonlocal arrangement, e.g. their period and lattice type. Here, we describe the optical properties of the gradient VA-SiNW samples and show that they display a rich combination of interesting optical phenomena that have not been comprehensively studied before and that are directly relevant for applications.

Figure 4a shows a reflectance spectrum (see Methods section of the SI for further details) taken at a position (x=9 mm) along the gradient, where the average center-to-center distance between the nanowires was Λ=395 nm (corresponding to the central AFM/SEM image in Figure 2a). Unlike in the case of previously examined 1µm-long vertically standing nanowires in arrays with a 1µm spacing, which produced single broad dips in reflectance[3] (~50-100 nm FWHM), we observed multiple sharp dips with a FWHM of ~20 nm. Figure 4b shows that these spectral features persist throughout the entire gradient VA-SiNW sample. In particular, the spectral dips appear at relatively constant spectral positions, become sharper for smaller nanowire separations and start to fade when the separations get close to ~350 nm. Moreover, for Λ approaching ~350 nm the sample no longer forms well-defined periodic arrangements of nanowires because the microgels enter into core-core contacts, leading to the formation of nanowire clusters (Fig. 2a for position x ≥ 16 mm) and fading of the reflection dips (Fig. 4b).

The observed features in the reflectance cannot be simply attributed to conventional interferences in thin films, but are related to the potential of the VA-SiNW to confine and guide light. To identify univocally the origin of these spectral features, we performed finite-difference-time-

domain simulations (FDTD) of the bright-field reflectance configuration (see Methods in the SI). Figure 4c and d show the simulated reflectance spectrum for Λ=400 nm, and, additionally, for varying separations between 350 and 500 nm, respectively. The simulated results agree with the features that appear in the experimental spectra of Figure 4a and b. Most importantly, they reproduce the multiple dips and their sharpening for smaller nanowire separations. The small differences observed between the simulations and experimental results stem from the experimental polydispersity of nanowire diameter and spacing, as for instance described by the error bars in Figure 2b or 3c, which lead to homogeneous broadening of the resonances. To support this claim further, in Figure 4e, we show a simulation of the reflectance vs. nanowire radius R for fixed nanowire separation Λ=400 nm. It can be seen that small changes in nanowire radius lead to large shifts in the spectral position of the multiple dips. . Additionally, surface roughness of the nanowires (see Methods section) may explain the lower experimental values of reflectance compared to the numerical simulations[39]. Roughness and slight polydispersity in the nanowire diameter may also be responsible for the fact that the fine features of the spectra in the short wavelength region (400-500nm) visible in the simulations are washed out in the experiments.

There are numerous reasons and optical phenomena that can lead to reflection dips. In the case of the examined VA-SiNW samples, with $L \approx 2.4$ μm, $R \approx 100$ nm, 350 nm $\leq \Lambda \leq$ 500 nm, the observed dips in normal incidence/reflection mode arise mainly from the coupling of incident light to Fabry-Perot resonances of the optical cavities that confine the light in the gaps between the nanowires and are supported by the coupled waveguide modes of the nanowires. To corroborate this conclusion, we show in Figure 4f-k plots of the simulated electric field around

the nanowires (see Methods in the SI) for the corresponding reflectance peaks and dips shown in Figure 4c. It can be seen that for the dips the field is confined in the gap between the nanowires and that for consecutive dips there are consecutive number of optical nodes in the gaps, which demonstrates the formation of Fabry-Perot cavity modes. The fact that these modes are supported by the nanowire waveguides is demonstrated nicely in Figure 4e where for thin nanowires there are no waveguide modes due to transverse cutoff of the modes, while for nanowires with larger radii the lowest order transverse waveguide modes start to appear and for even larger nanowire radii the signature of higher order transverse modes emerges. Finally, since the dips are Fabry-Perot resonances, a dip is observed whenever the wavelength the cavity λ_q is an integer multiple of the cavity roundtrip length: $\lambda_q=2*L/k$ where k is an integer number and $\lambda_q= \lambda_0/n_{eff}$, where λ_0 is the light wavelength in vacuum and n_{eff} is the effective refractive index of the Si nanowires. The cavity in our sample, i.e. the nanowires, is long enough in order to meet this criterion several times for the spectrum of a Xenon lamp. This effect can be seen also in the simulations data reported in Figure 4 f-h.

In addition to complex reflectance, ordered nanostructured materials can also lead to strong scattering of light and creation of vivid structural colors due to photonic crystals that are formed in the materials. This phenomenon can also be observed in nature as a coloring mechanism, e.g, for certain types of insects, butterflies and birds [39] and it is evident in Figure 2d. To characterize this effect in our samples, we measured the back-scattering of white light from a tilted gradient sample. Illustration of the experimental configuration is shown in Figure 5a (see Methods in the SI). Due to the gradually varying spacing between the nanowires, different regions in the sample back-scatter light at different wavelengths and Figure 5b shows a color photograph of the back-

scattering for θ=54°. It can be seen that the backscattering changes with position along the gradient and that it shifts from blue to red (See also Supplementary Figure S5 for additional details). Figure 5c shows the corresponding normalized spectral measurements as a function of position on the sample in Figure 5b using an imaging spectrometer. In this case, contrary to the bright field normal reflection case, we observed only one reflection peak that shifts to shorter wavelengths with decreasing center-to-center spacing between nanowires. The results nicely fit the prediction for light diffraction of 2D hexagonal lattice photonic crystals [40] with a gradient in spacing

$$\Lambda(x)=\frac{\lambda(x)}{\sqrt{3}\sin(\theta)}(1)$$

where λ is the position-dependent peak diffracted wavelength in free space (Equation 1). The calculated center-to-center distance is shown as the top axis in Figure 5c and can be directly compared to the one measured with SEM (white circles), demonstrating that indeed the samples behaves as a tunable 2D photonic crystal.

In addition to the features reported above, a unique aspect of our Soft Nanoparticle Templating approach is the easy integration with other existing parallel patterning techniques. In particular, the combination with standard optical lithography enables the fabrication of large-scale microstructured patterns of VA-SiNWs using the same process flow (see Methods in the SI for more details). This combined lithography relies on the strong adhesion of the soft nanoparticles on the silanized silicon substrates, fixing the microgel array during the optical lithography steps, in which a photoresist pattern is created on top of the microgels. The exposed particles are entirely removed by oxygen plasma, while the protected ones stay intact. Subsequent rinsing

with acetone and ethanol, as previously described, exposes and swells the initially protected microgels, enabling the fabrication of the hierarchical lithography masks that define micropatterned arrays of VA-SiNWs, as demonstrated in Figure 6 (see also Supplementary Figure S6 for additional details). Three examples of such structures with circular, linear and triangular micropatterns are shown.

We have demonstrated that harnessing the self-assembly of microgels at fluid (o/w) interfaces enables a novel nanoscale patterning paradigm that addresses and overcomes current bottlenecks in the fabrication of fully tunable VA-SiNW arrays over large areas. In particular, the continuous and simultaneous compression and deposition of interfacial monolayers of microgels enable us to produce a customized lithographical mask to grow VA-SiNW arrays with adaptable and programmable designs by means of MACE. Importantly, this approach enables independent control over spacing and diameter of the nanowire elements, defined by the deposition protocol and the microgel size. This feature was exploited for the fabrication of VA-SiNW arrays with gradients in spacing and constant diameter. Future work with differently sized microgels will extend the range of available geometrical parameters. Our fully tunable samples show extremely rich optical behavior in the visible range, in particular via the formation of controlled optical cavities that confine the optical fields to the gaps between the NWs and thus can potentially be used as for sensing, stimulated emission and nonlinear optics applications. Finally, the possibility to produce hierarchical patterns of VA-SiNWs paves the way for new applications in optical circuits, complex platforms for cell studies and surfaces with programmable adhesion and wettability.

FIGURES

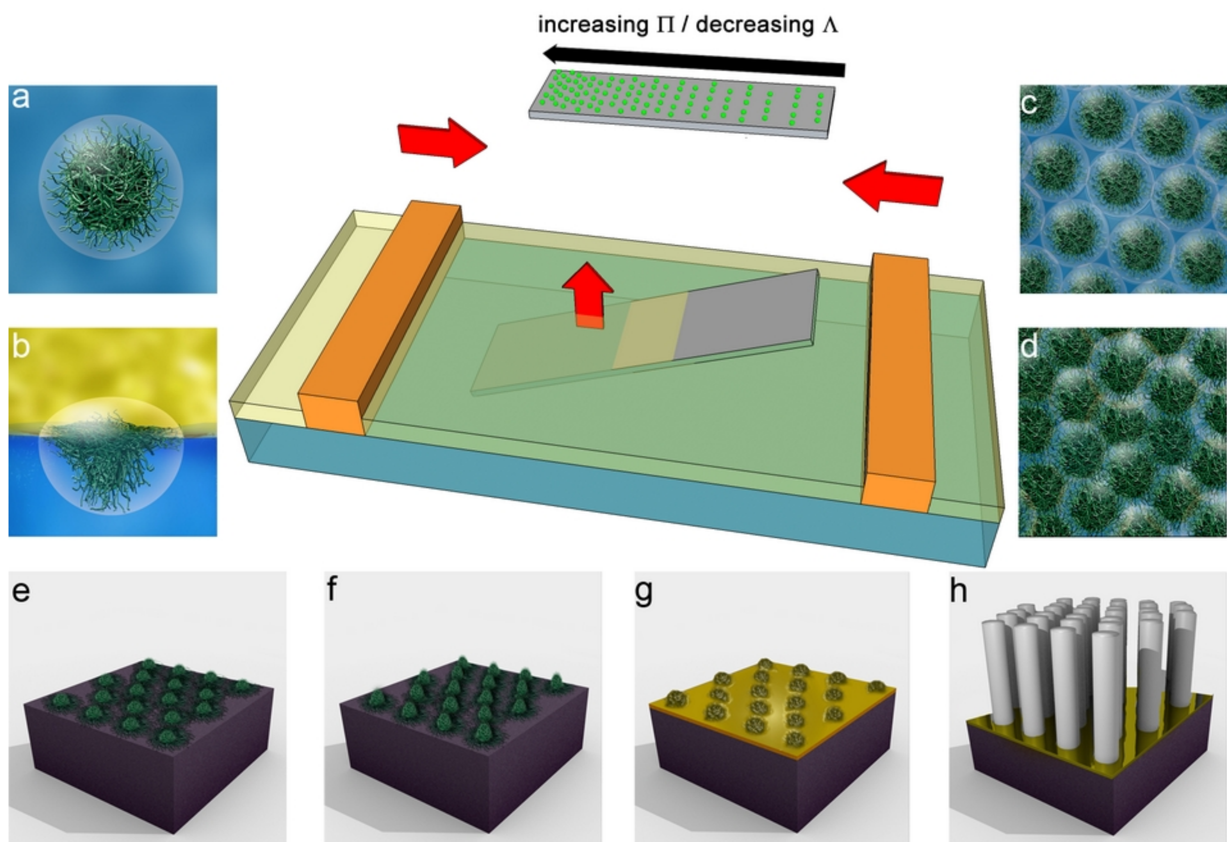

Figure 1. Schematics of the Soft Nanoparticle Templating process. The central element shows the workings of the experimental setup. The o/w Langmuir trough is schematically drawn, showing the two barriers used to compress the interface. Simultaneous to interface compression, a silicon wafer is lifted through the interface at an angle of 30° and then emerges through the oil-air interface. The process produces a gradient in spacing of the deposited microgels, as schematically shown on the substrate after lift-off. a-b) Schematic representation of microgel particles in bulk water and at an oil-water interface, respectively. The core-shell nature of the particles is displayed, together with their deformation and flattening at the o/w interface. c-d) Top view of the microstructure of the microgel monolayer at different degrees of compression. The steric contacts between the coronas at the interface are compressed giving rise to hexagonal particle lattices with gradients in the interparticle spacing. Different positions on the silicon substrate correspond to different degrees of compression, with decreasing particle separation from ight to left, corresponding to increasing surface pressure. Bottom row: main steps of the VA-SiNW array fabrication via MACE. The deposited microgel array (e) is swollen in photoresist, leading to an increased particle height from the substrate (f). A 10 nm-layer of Au is deposited (g) and the microgels provide masking for the contact between the Au layer and the Si substrate. Upon exposure to the etching solution, the MACE reaction proceeds around the swollen microgels, causing the formation of VA-SiNWs that replicate the lateral geometry of the customized microgel shadow mask with high fidelity (h).

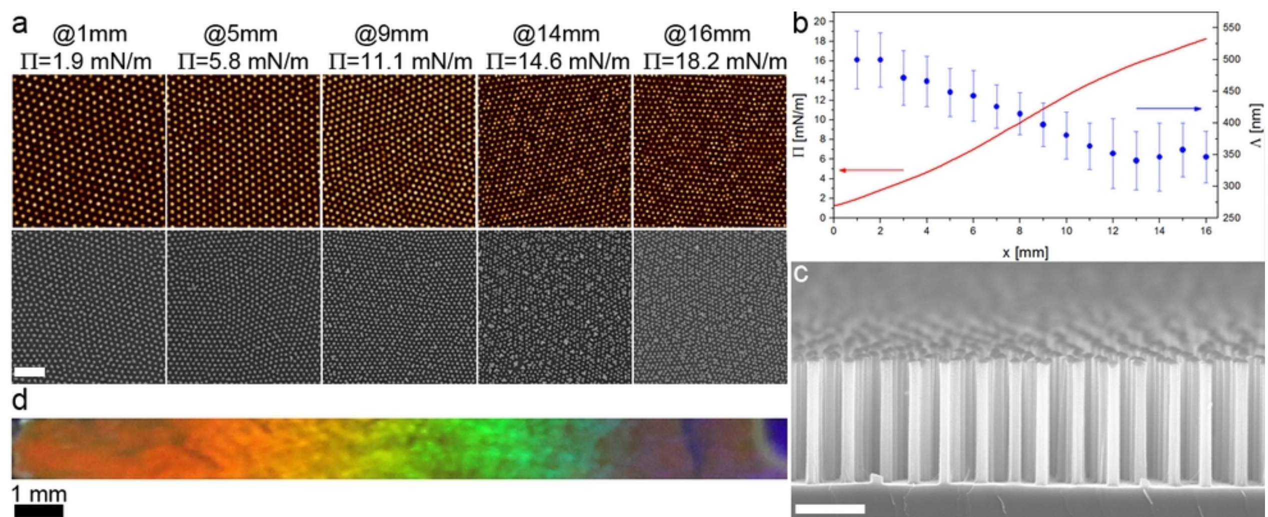

Figure 2. Characterization of gradient samples. a) 10x10 μm^2 AFM images of deposited microgels and corresponding top-view SEM micrographs of the VA-SiNW arrays taken at different positions along a gradient sample, corresponding to the surface pressures reported above each image. Scale bar 2μm for all images. b) Center-to-center nanowire separation Λ and corresponding surface pressure Π as a function of position x on the substrate. Compression proceeds from left to right, causing a progressive and controlled reduction of nanowire separation. c) SEM cross-section of the VA-SiNW array with a height of 1.8 μm and average radius of 90 nm (aspect ratio 20). Scale bar 1 μm. d) Optical photograph of the gradient sample

showing continuously varying structural colors across the whole visible spectrum on a single substrate.

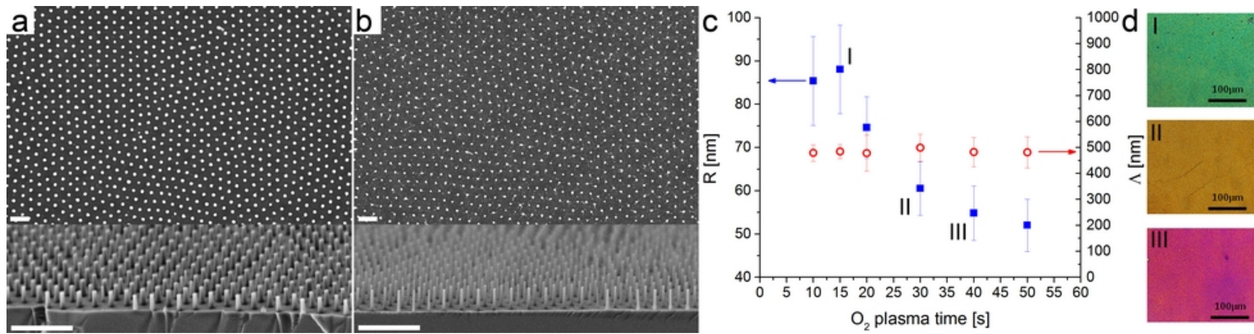

Figure 3. Control over nanowire diameter. a-b) Top-view (scale bar 1 μm) and cross-section (scale bar 2 μm) SEM micrographs of VA-SiNWs from microgel masks obtained after 15 and 40 s O_2 plasma etching, respectively. c) nanowire radius R and center-to-center nanowire spacing Λ as a function of exposure time to oxygen plasma. The nanowire radius can be tuned independently of the nanowire separation. d) Bright-field optical photographs at normal incidence corresponding to data points I, II and III on the graph, in which the etched VA-SiNW arrays show vivid colors.

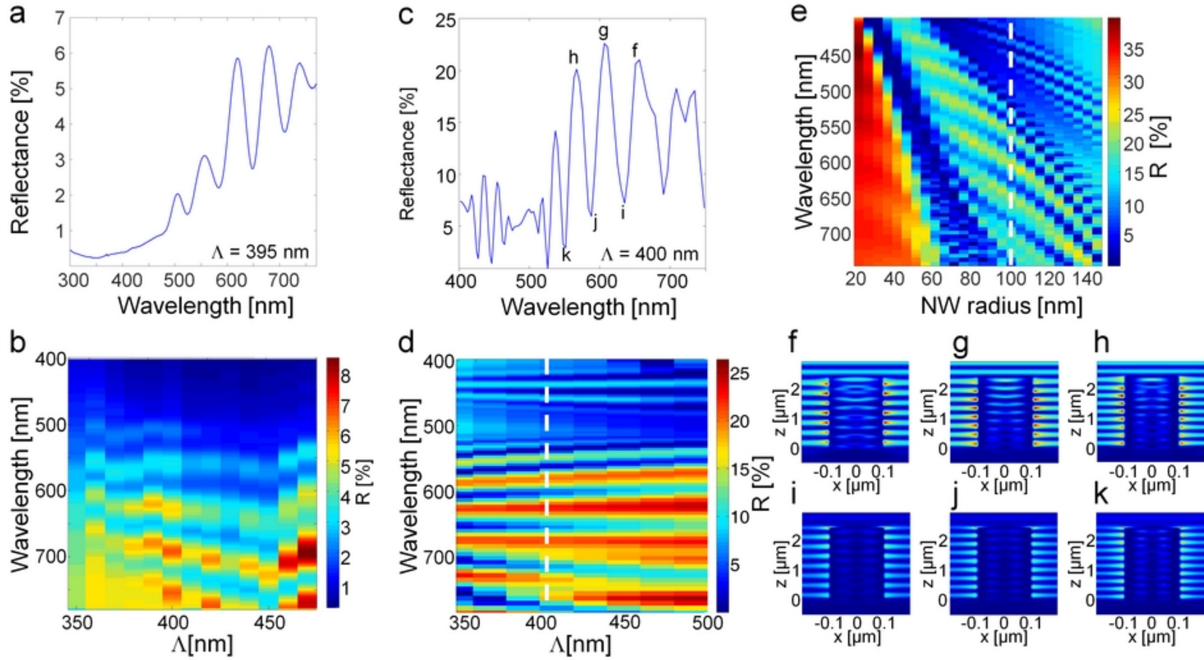

Figure 4. Large-scale formation of nanowire-supported optical cavities with multiple resonances. a) Bright-field reflectance spectra for VA-SiNW taken at a position with average nanowire separation Λ=395nm. b) Reflectance spectra taken at different positions along the sample vs. the measured average local nanowire spacing Λ. c) Simulated reflectance spectra for Λ=400nm. Nanowire radius is 100nm and nanowire length is 2.4μm. d-e) Simulated reflectance spectra vs. nanowire spacing (radius 100nm) (d) and nanowire radius (spacing 400nm) (e). The vertical dashed lines correspond to the spectra in (c). f-k) Simulations of normalized magnitude of the electric fields in a single unit cell for spectral peaks at 656nm (f), 606nm (g) , 567nm (h) and for spectral dips at 635nm (i), 588nm (j), and 551nm (k). The electric field shows confinement of light due to formation of optical cavities in the dip positions with consecutive number of nodes (8 in i, 9 in j and 10 in k).

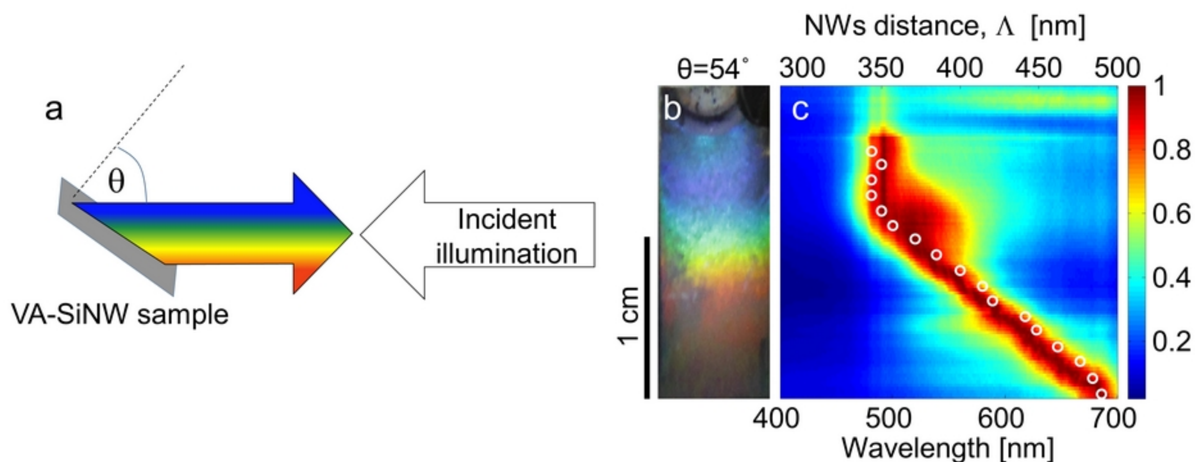

Figure 5. Colored backscattering due to formation of tunable gradient spacing, large scale, hexagonal photonic crystal. a) Illustration of backscattering measurement scheme. b) Color photograph of position-dependent backscattering from the gradient spacing sample. The grey semicircle at the top marks the position of the sample holder during microgel deposition. The colors range corresponds to surface pressures between 2 mN/m and 18 mN/m going from the largest spacing (red) to the smallest one (blue). c) Normalized, position-dependent, backscattering spectra form the sample in (b). The top axis is the average NWs separation calculated from Eq. 1, which corresponds to the measured wavelength axis (bottom). The white circles are local center-to-center distances between nanowires (Λ) measured with SEM.

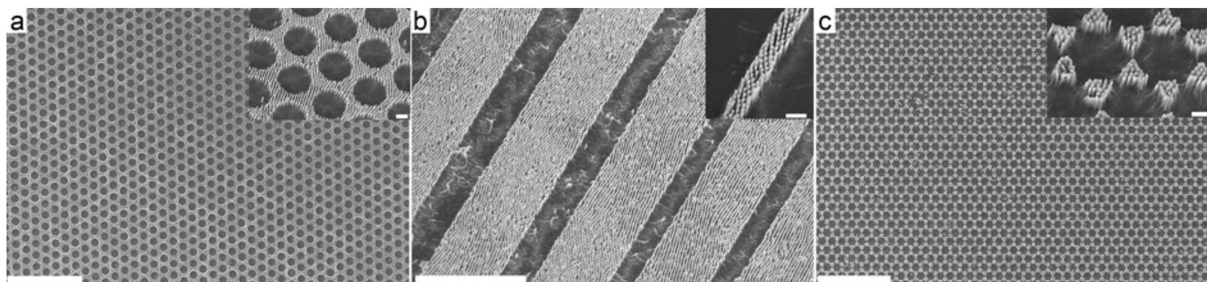

Figure 6. Hierarchical structures from combined lithography. a-c) Examples of hierarchical, micropatterned VA-SiNW arrays from combined SNT and photolithography. a) Scale bar 50 µm; b) Scale bar 20 µm; c) Scale bar 50 µm. The scale bars in the insets correspond to 1µm.

ASSOCIATED CONTENT

Supporting Information. The Supporting Information contain all the experimental details in the a Methods Section plus additional figures and data. This material is available free of charge via the Internet at http://pubs.acs.org.

AUTHOR INFORMATION

Corresponding Author

*Lucio Isa. Email: lucio.isa@mat.ethz.ch

Author Contributions

†These two authors contributed equally to this work.

LI designed the study. MR, RE, NHV, MAFR, MZ and LI performed the substrate fabrication, the microscopy measurements and the corresponding data analysis. RD and TE performed the optical characterization and the numerical simulations. KG and WR synthesized the microgel particles. MR and AF did the optical lithography and swelling of the particles. VVN and MR did the IR measurements and analysis. All authors contributed to the discussion and wrote the paper.

ACKNOWLEDGMENT

LI would like to thank Prof. N.D. Spencer, Prof. A. Studart and Prof. J. Vörös for access to instrumentation. LI and MZ acknowledge financial support from the Swiss National Science Foundation grant PP00P2_144646/1. NHV kindly acknowledges fellowship support from the Alexander von Humboldt Foundation. MAFR acknowledges financial support from the COST action: Smart and Green Interfaces (STSM MP1106-14761) and would like to thank Prof. R. Hidalgo-Alvarez, Prof. M.A. Rodriguez-Valverde and Prof. M.A. Cabrerizo-Vilchez for supporting his COST fellowship. KG and WR acknowledge financial support from the German Research Foundation within the Collaborative Research Center SFB985 "Functional Microgels and Microgel Systems". TE acknowledges financial support from the European Commission Marie Curie Career Integration Grant (grant no. 333821). Marc Cirera is acknowledged for the illustrations in Figure 2a-h.

REFERENCES

(1) Robinson, J. T.; Jorgolli, M.; Shalek, A. K.; Yoon, M.-H.; Gertner, R. S.; Park, H. *Nat Nano* **2012**, *7*, 180.

(2) Park, H.; Crozier, K. B. *Sci. Rep.* **2013**, *3*.

(3) Seo, K.; Wober, M.; Steinvurzel, P.; Schonbrun, E.; Dan, Y.; Ellenbogen, T.; Crozier, K. B. *Nano Lett.* **2011**, *11*, 1851.

(4) Peng, K.; Jie, J.; Zhang, W.; Lee, S.-T. *Applied Physics Letters* **2008**, *93*, 033105.

(5) Krivitsky, V.; Hsiung, L.-C.; Lichtenstein, A.; Brudnik, B.; Kantaev, R.; Elnathan, R.; Pevzner, A.; Khatchtourints, A.; Patolsky, F. *Nano Lett.* **2012**, *12*, 4748.

(6) Chiappini, C.; De Rosa, E.; Martinez, J. O.; Liu, X.; Steele, J.; Stevens, M. M.; Tasciotti, E. *Nat Mater* **2015**, *14*, 532.

(7) Park, H.; Crozier, K. B. *ACS Photonics* **2015**, *2*, 544.

(8) Goldberger, J.; Hochbaum, A. I.; Fan, R.; Yang, P. *Nano Lett.* **2006**, *6*, 973.

(9) Cuevas, A.; Dalchiele, E. A.; Marotti, R.; Leinen, D.; Ramos-Barrado, J. R.; Martin, F. *Journal of Materials Research* **2011**, *26*, 1091.

(10) Min, W.-L.; Jiang, B.; Jiang, P. *Adv. Mater.* **2008**, *20*, 3914.

(11) Elnathan, R.; Kwiat, M.; Patolsky, F.; Voelcker, N. H. *Nano Today* **2014**, *9*, 172.

(12) Garnett, E.; Yang, P. *Nano Lett.* **2010**, *10*, 1082.

(13) Walia, J.; Dhindsa, N.; Khorasaninejad, M.; Saini, S. S. *Small* **2014**, *10*, 143.

(14) Shalek, A. K.; Robinson, J. T.; Karp, E. S.; Lee, J. S.; Ahn, D.-R.; Yoon, M.-H.; Sutton, A.; Jorgolli, M.; Gertner, R. S.; Gujral, T. S.; MacBeath, G.; Yang, E. G.; Park, H. *Proceedings of the National Academy of Sciences* **2010**, *107*, 1870.

(15) Morales, A. M.; Lieber, C. M. *Science* **1998**, *279*, 208.

(16) Lu, W.; Lieber, C. M. *Journal of Physics D: Applied Physics* **2006**, *39*, R387.

(17) Law, M.; Goldberger, J.; Yang, P. *Annual Review of Materials Research* **2004**, *34*, 83.

(18) Park, W. I.; Yi, G. C. *Adv. Mater.* **2004**, *16*, 87.

(19) Dick, K. A.; Deppert, K.; Mårtensson, T.; Mandl, B.; Samuelson, L.; Seifert, W. *Nano Lett.* **2005**, *5*, 761.

(20) Han, H.; Huang, Z.; Lee, W. *Nano Today* **2014**, *9*, 271.

(21) Huang, Z.; Geyer, N.; Werner, P.; de Boor, J.; Gösele, U. *Adv. Mater.* **2011**, *23*, 285.

(22) Li, X. *Current Opinion in Solid State and Materials Science* **2012**, *16*, 71.

(23) Hochbaum, A. I.; Fan, R.; He, R.; Yang, P. *Nano Lett.* **2005**, *5*, 457.

(24) Pevzner, A.; Engel, Y.; Elnathan, R.; Ducobni, T.; Ben-Ishai, M.; Reddy, K.; Shpaisman, N.; Tsukernik, A.; Oksman, M.; Patolsky, F. *Nano Lett.* **2010**, *10*, 1202.

(25) Salaita, K.; Wang, Y.; Mirkin, C. A. *Nat Nano* **2007**, *2*, 145.

(26) Mårtensson, T.; Carlberg, P.; Borgström, M.; Montelius, L.; Seifert, W.; Samuelson, L. *Nano Lett.* **2004**, *4*, 699.

(27) Højlund-Nielsen, E.; Weirich, J.; Nørregaard, J.; Garnaes, J.; Asger Mortensen, N.; Kristensen, A. *NANOP* **2014**, *8*, 083988.

(28) Amanti, M. I.; Bismuto, A.; Beck, M.; Isa, L.; Kumar, K.; Reimhult, E.; Faist, J. *Opt. Express* **2013**, *21*, 10917.

(29) Reimhult, E.; Kumar, K.; Knoll, W. *Nanotechnology* **2007**, *18*, 275303.

(30) Vogel, N.; Goerres, S.; Landfester, K.; Weiss, C. K. *Macromolecular Chemistry and Physics* **2011**, *212*, 1719.

(31) Isa, L.; Kumar, K.; Müller, M.; Grolig, J.; Textor, M.; Reimhult, E. *ACS Nano* **2010**, *4*, 5665.

(32) Ray, M. A.; Jia, L. *Adv. Mater.* **2007**, *19*, 2020.

(33) Xia, Y.; Yin, Y.; Lu, Y.; McLellan, J. *Advanced Functional Materials* **2003**, *13*, 907.

(34) Li, X.; Wang, T.; Zhang, J.; Yan, X.; Zhang, X.; Zhu, D.; Li, W.; Zhang, X.; Yang, B. *Langmuir* **2010**, *26*, 2930.

(35) Guillermo, A.; Cohen Addad, J. P.; Bazile, J. P.; Duracher, D.; Elaissari, A.; Pichot, C. *Journal of Polymer Science Part B: Polymer Physics* **2000**, *38*, 889.

(36) Stieger, M.; Richtering, W.; Pedersen, J. S.; Lindner, P. *The Journal of Chemical Physics* **2004**, *120*, 6197.

(37) Geisel, K.; Isa, L.; Richtering, W. *Langmuir* **2012**, *28*, 15770.

(38) Geisel, K.; Richtering, W.; Isa, L. *Soft Matter* **2014**, *10*, 7968.

(39) Vukusic, P.; Sambles, J. R. *Nature* **2003**, *424*, 852.

(40) Kittel, C. *Introduction to Soli State Physics, 8th Edition* Wiley, 2005.

Insert Table of Contents Graphic and Synopsis Here

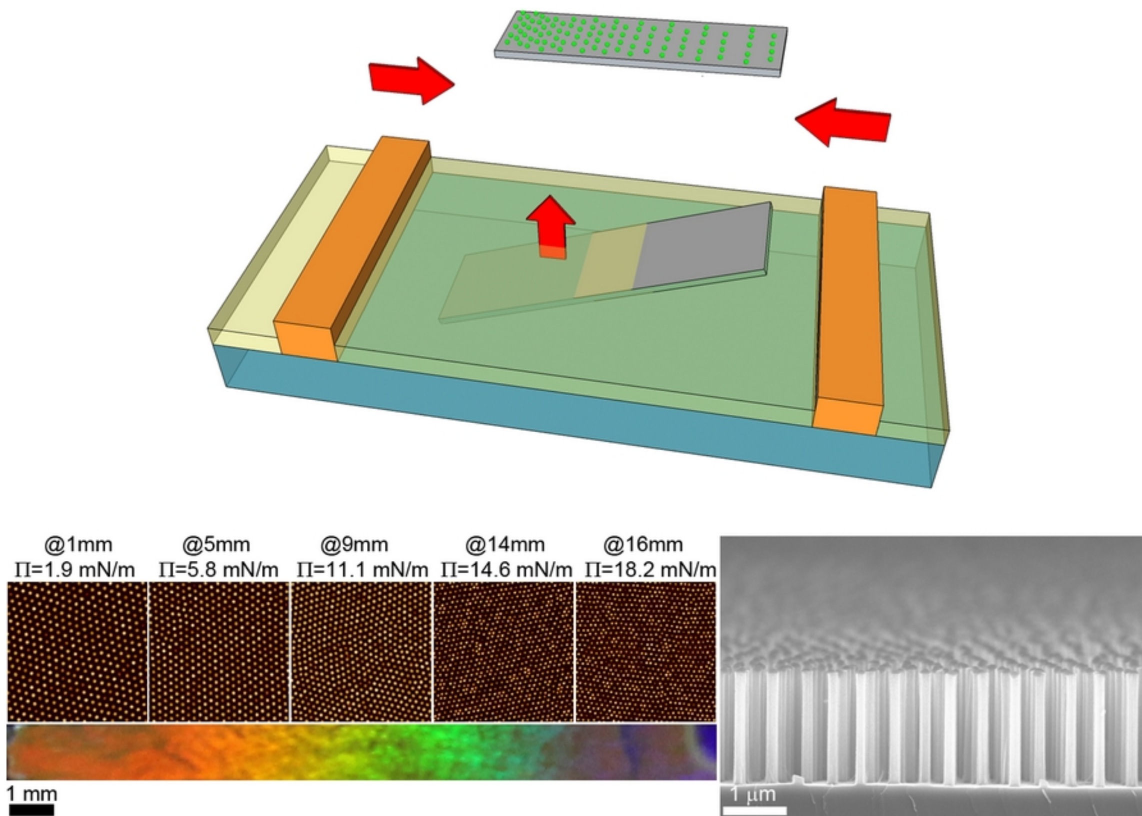

Schematic representation of the Soft Nanoparticle Templating process to produce fully tunable, optically active arrays of vertically aligned silicon nanowires.